Influence of the incident radiation on the energy performance of two small-scale solar Organic Rankine Cycle trigenerative systems: a simulation analysis

Mauro Villarini[a1], Roberto Tascioni[b,d], Alessia Arteconi[c,d], Luca Cioccolanti[d]

[a] Tuscia University of Viterbo, Via San Camillo de Lellis, snc , 01100 – Viterbo, Italy. Email: mauro.villarini@unitus.it
[b] Department DIAEE, Sapienza University of Rome, Via Eudossiana 18, Rome, Italy. Email: roberto.tascioni@uniroma1.it
[c] DIISM, Università Politecnica delle Marche, via brecce bianche, 1 60131 Ancona, Italy. Email: a.arteconi@univpm.it
[d] Università Telematica e-Campus, Via Isimbardi 10, 22060 - Novedrate, CO, Italy. Email: alessia.arteconi@uniecampus.it; roberto.tascioni@uniecampus.it; luca.cioccolanti@uniecampus.it

Abstract

In this paper, two innovative small-scale solar Organic Rankine Cycle (ORC) trigeneration plants are investigated and compared using a simulation analysis. In particular, the first plant (Plant 1) consists of a 146 m^2 Compound Parabolic Collectors (CPC) solar field, a 3m^3 diathermic oil storage tank, a 3.5 kWe ORC plant and a 17 kWc absorption chiller, while the second plant (Plant 2) consists of a Linear Fresnel Reflectors (LFR) solar field of equal reflecting area, a phase change material storage tank equipped with reversible heat pipes, a 3.2 kWe ORC unit and the same 17 kWc absorption chiller as the former.
The dynamic performance of the considered plants has been assessed for two Italian locations, Napoli and Messina, having a similar global radiation but a significantly different ratio of direct normal irradiance to diffuse irradiance. The comparison between the two different solar ORC trigeneration systems has revealed the great influence of the solar radiation on the effectiveness of such systems even for locations at similar latitudes. The energy production has been analysed both on a monthly and daily basis. Results have shown that while the performance of Plant 1 is not so sensitive to location and radiation conditions, Plant 2 is greatly affected by these parameters. Moreover, the higher condensing temperatures necessary in summer to supply the absorption chiller significantly limit the electrical efficiency of the solar CPC ORC. On the contrary, the LFR technology allows to achieve higher temperatures and conversion efficiencies in summer, thus resulting especially suitable for solar cooling applications. In conclusion, this study has highlighted the importance of adequate technology selection with different radiation conditions in order to better exploit the potential of trigenerative solar ORC systems.

Keywords

renewable energy; concentrated solar power technologies; ORC system; thermal energy storage; trigeneration; micro-combined cooling heating and power system

[1] Corresponding Author

Nomenclature

A	area of the collector [m^2]
a_0	first order efficiency coefficient [$W/m^2 \cdot K$]
a_1	second order efficiency coefficient [$W/m^2 \cdot K$]
CCHP	Combined Cooling, Heating and Power
COP	Coefficient Of Performance
CPC	Compound Parabolic Collector
CSP	Concentrated Solar Power
DNI	Direct Normal Irradiation [W/m^2]
ETC	Evacuated Tube Collector
G_b	direct radiation on collector plane [W/m^2]
G_d	diffuse radiation on collector plane [W/m^2]
h_{abs}	operating hours of the absorption chiller [h]
h_{ORC}	operating hours of the ORC unit [h]
HSW	hot sanitary water
HTT	High Temperature storage Tank
IAM	Incident Angle Modifier
LCOE	Levelized Cost Of Energy
LFR	Linear Fresnel Reflector
LTT	Low Temperature storage Tank
NZEB	Nearly Zero Energy Buildings
K_θ	Incident Angle Modifier for direct radiation
K_d	Incident Angle Modifier for diffuse radiation
$\dot{m}_c$	mass flow rate of the cooling water [kg/s]
$\dot{m}_f$	mass flow rate of the organic fluid [kg/s]
NTU	Number of Transfer Units
OM	Operation Mode of Plant 2
P1	Plant n.1
P2	Plant n.2
P_e	Electrical Power [kWe]
P_c	Cooling Power [kWc]
P_t	Thermal Power [kWt]
P_{abs}	cooling power output from the absorption chiller [kW_c]
$P_{abs,in}$	thermal power input to the absorption chiller[kW_t]
$P_{ORC,el}$	electrical power produced by the ORC unit [kW_e]
$P_{ORC,out}$	outlet thermal power from the ORC unit [kW_t]
$P_{ORC,in}$	inlet thermal power to the ORC unit [kW_t]
$P_{SF,in}$	inlet power to the solar field [kW]
$P_{SF,out}$	outlet thermal power from the solar field [kW_t]
PCM	Phase Change Material
PTC	Parabolic Trough Collector
Q_{loss}	heat losses at the receiver [kW_t]
Q_{PCM}	heat exchanged by the PCM [kW_t]
R_{irr}	ratio of DNI to diffuse irradiance
SM	Solar Multiple
TES	Thermal Energy Storage
T_a	ambient air temperature [°C]
T_{av}	average temperature [°C]
T_{in}	inlet temperature of the cooling water at the condenser [°C]
T_m	mean temperature of the fluid in the collector [°C]
T_{out}	outlet temperature of the cooling water at the condenser [°C]
$T_{ORC,off}$	lower bound temperature set-point of the TES [°C]
$T_{ORC,on}$	upper bound temperature set-point of the TES [°C]
$T_{TES,av}$	average temperature of the TES [°C]
Δh_e	actual specific enthalpy difference across the expander [kJ/(kg K)]
Δh_p	actual specific enthalpy difference across the pump [kJ/(kg K)]

ΔT_h	hot period working temperature range of HTT-ORC inlet [°C]
ΔT_c	cold period working temperature range of HTT-ORC inlet [°C]
ΔT_m	mid seasons working temperature range of HTT-ORC inlet [°C]
ΔT_{PCM}	temperature difference between the PCM and the heat transfer medium [°C]
$\Delta t_{int\text{-}timestep}$	time interval of the internal time step [s]

Greek symbols

α	solar elevation angle
β	absorptance coefficient
ε	emittance coefficient
η_{el}	electrical efficiency
$\eta_{e,ORC}$	ORC unit electrical efficiency
$\eta_{glob,CCHP}$	CCHP global efficiency
η_m	mechanical efficiency
η_{opt}	optical efficiency
$\eta_{opt,max}$	maximum optical efficiency
$\eta_{ORC,el}$	ORC unit electrical efficiency
$\eta_{ORC,th}$	ORC unit thermal efficiency
η_{REC}	receiver efficiency
η_{SF}	overall conversion efficiency of the solar field
η_{TES}	TES efficiency
σ	solar azimuthal angle
θ	solar incident angle

1. Introduction

The rise of global energy demand connected in particular with the growing population and the progress of developing countries requests huge amounts of energy resources making their diversification crucial. In Europe, instead, nearly 80% of the energy use relies on foreign reservoirs, fact that undermines the security of the energy supply.

Therefore, it becomes more and more important to make use of locally available renewable sources all over the world. Among them, solar is one of the most remarkable with great potential at residential level, which in turn represents 25.4 % of final energy end-use in European Union [1]. The implementation of NZEB is expected to significantly contribute to minimize the greenhouse gas emissions of the sector, thus mitigating the climate change phenomena. In these buildings, the low amount of energy required is provided mostly by renewables, especially by solar technologies [2]. Pietzcker et al. in [3] have considered solar power as the potential dominant source of electricity in a 2010-2100 scenario limiting global warming to 2° C and have shown that the application of solar technologies has stabilizing effects on electricity prices. Among the different solar technologies, Concentrated Solar Power (CSP) is increasing its attractiveness also for residential applications and it has been already considered by many researchers, particularly for remote and off grid installations. CSP consists in the concentration of the solar radiation into a smaller area in order to achieve higher temperature levels compatible with more sophisticated applications than the mere domestic use of heat, as e.g. industrial processes, power generation, cooling. The potential of CSP for power generation, with an overall capacity of 5 GW achieved in 2014 [4], allows to consider a positive scenario in the next decades both for Africa and Europe [5], whose adoption has been supposed by means of projects like Desertec [6]. In that direction, the evolution of an effective transfer system, as point-to-point High Voltage Direct Current, of CSP solar power from desert region to important metropolitan area and, in particular, from MENA (Middle East and North Africa) to Europe will have beneficial impact on the global energy system [7]. Moreover China, which represents the leading energy exploiter nowadays [8], is seriously operating in order to respect the target fixed by the Paris Agreement and it is planning to install at least 54 GW of solar plants, encompassing concentrated solar power and solar photovoltaic [9]. Taking into account that the energy policies adopted by China from 2007 onwards have brought solar photovoltaic panels to their maturity and significantly reduced the related levelized cost of energy (LCOE) [10], a similar development is expected to occur also for CSP technologies. In the last years, the potential of CSP technologies, even at small scale, has been recognized both for combined heat and power (CHP) and combined cooling heat and power (CCHP) applications [11] and it is especially appreciated in areas inadequately served by conventional power stations, where off-grid poly-generation systems are more advantageous than extending a power line (whose cost ranges from $15,000 to $50,000 per mile) [12].

The literature review carried out has shown a rising interest towards design, test and optimization of these systems. Different configurations have been considered both with respect to the solar collectors and the final use of the solar energy input. With respect to the different ways of collecting the solar radiation, five CSP technologies are available at present: Parabolic Trough Collector (PTC), Solar Power Tower (SPT), Parabolic Dish System (PDS), Linear Fresnel Reflector (LFR) and Compound Parabolic Collector (CPC) [13]. The concentration ratio and the overall performance of such technologies significantly differ from each other also due to the solar radiation that each system is able to collect. Parabolic Trough Collector is one of the most performing CSP technology with many applications [14]. Solar Power Tower is a very promising technology as well: the direct solar radiation is focused on a receiver located on the top of a tower [15]. However, both these technologies are particularly used for large-size power generation. Dish systems consist of a paraboloid dish concentrator that collects energy into a central cavity receiver [16]. Such systems have a very high potential in terms of conversion efficiency, but are the less commercially advanced among the CSP technologies at present. Linear Fresnel Reflector is a line-focus CSP technology as PTC and is becoming more and more important for both industrial heating and electricity generation [17]. Differently from the other CSP technologies, LFR has a lower impact in terms of cost of technology, thanks to a lighter and simpler structure [18]. Finally, Compound Parabolic Collector is able to collect both direct and diffuse solar radiation without a tracking system and it proved to be a suitable option due to its low cost and good thermal performance at low and medium temperature ranges [19].

In combination with CSP technologies, Organic Rankine Cycle systems are usually adopted at small scale [20–22] to efficiently convert the solar energy into power. Several studies in literature [23,24] have been focused on the application of ORC systems driven by CSP. For example, Freeman et al. [25] and Desai et Bandyopadhyay [26] have focused their attention on the proper selection of working fluids for solar ORC. Similarly Freeman et al. [27] focused their attention on a small scale combined heat and power system for domestic use in UK and compared the performance of the same total array area composed of PTC and ETC. Quolin et al. [28] designed the main components of a low-cost solar ORC with particular focus on the scroll expander [28] and compared its performance with those of two different expansion machines by varying the working fluids. Furthermore, Casartelli et al. [29], after the selection of the most proper working fluid of a 5 MW ORC unit powered by linear solar collectors, studied the market parity for two different off-design control strategies with respect to two different linear CSP technologies: parabolic trough collector and linear Fresnel reflector. Other works [30,31] put on evidence the application of solar ORC plants in remote areas and off-grid context to feed a reverse osmosis desalination system for fresh water production.

However, to the best of the authors' knowledge, only few articles in literature have studied CSP solar systems coupled with ORC plants for trigeneration purposes by means of an absorption chiller. Compared to CCHP plants using electric chillers, thermally driven absorption chillers require a lower amount of electric energy and can exploit the huge amount of medium temperature thermal energy collected by the solar field during the summer season. At large scale, Mehrpooya et al [32] carried out a simulation analysis in Aspen Hysys of a solar thermal power plant consisting of parabolic dish solar collectors and steam turbine coupled with a multi-effect desalination plant and a single-effect absorption chiller. In particular, they obtained a production of 4,632 kWe, 820.8 kWc and a 22.79 kg/s flow rate of fresh water with a 66.05% exergy efficiency of the multigeneration system. At small scale, Boyaghchi et Heidarnejad [33] performed a thermoeconomic analysis and a multi-objective optimization of a novel solar powered trigeneration system based on a 2.7 kWe ORC unit for electricity production and an ejector refrigeration cycle for cooling during summer. Karellas and Braimakis developed a thermodynamic model and an economic analysis of a trigeneration system based on the operation of an ORC and a vapor compression cycle powered by a biomass boiler and a solar PTC [34]. Some of the authors have been studying solar powered ORC systems in last years [35] and in a previous work studied the main technical aspects and economic benefits of a CCHP solar system [36], consisting of a 50 m^2 CPC solar field, a 3.5 kWe ORC unit and a 17.6 kWf absorption chiller. In particular, it was proved that a proper setting of the system, in terms of temperature operating ranges, can be very effective to increase the overall energy produced by the CCHP system. However, they also found that an adequate size of the solar field area is of paramount importance to achieve a significant energy production and exploit the ORC system at its best.

In this paper, the energy performance of the trigeneration plant previously analyzed by the authors has been evaluated in two different locations in Italy and compared to a similar trigeneration system based on the prototype conceived in the Innova MicroSolar Horizon 2020 research project [37], where LFR is used for the solar field. The main novelties of the present paper rely on: (i) the investigation of two solar systems, that are going to be experimentally tested in the near future, interesting for the innovative combination of small-scale and CCHP set-up; (ii) the evaluation of the effect of direct beam radiation on the performance of the two trigeneration systems based on solar technologies with different concentration ratio and operating temperature. The Direct Normal Irradiance (DNI), as a component of the Global Horizontal Irradiance (GHI), indeed, has been demonstrated to be a decisive factor for the design of solar systems [38]. Furthermore, distribution and magnitude of DNI is very dependent on the atmospheric contents, cloud amounts and precipitation level as shown by Mohammadi and Goudarzi [39], generating consequences on performance and continuity of CSP systems. In the present work, the performance of the two mentioned CCHP systems has been comparatively evaluated in two distinct locations with the same Global Horizontal Irradiance differently distributed between Direct Normal Irradiance and Diffuse Horizontal Irradiance (DHI).

Hence, the paper is organized as follows: after the Introduction, the Methodology is presented and after that a description of the two plants considered in this analysis is provided. In Section 4 the models of the plants are described, while Section 5 reports the results of the analysis. The last section, finally, reports the main conclusions.

2. Methodology

In this paper two specific plants are considered: a CPC-ORC trigenerative prototype (Plant 1) and a LFR-ORC trigenerative prototype (Plant 2). The configuration of the systems under analysis has been defined in order to perform a fair comparison between them, taking into account their peculiarities highlighted by the results obtained from previous studies [36,40]. In detail, with reference to Plant 1, because of the fundamental effect of the solar field on the overall energy production of the system [36], its original size has been increased and the same collecting area of the LFR-ORC prototype plant of the Innova MicroSolar project [37], which corresponds to about 146 m^2, assumed in this work. As regards Plant 2, instead, it has been coupled with the same absorption chiller of Plant 1, in order to evaluate its performance in trigenerative configuration.

Because of their intrinsic operation, CSP systems are appropriate at latitudes where the radiation is high. In Europe, Southern countries, such as Italy, are expected to give a significant contribution to their development and optimization. Therefore, in order to better estimate the influence of the available solar irradiance on the performance of both plants, two different locations with the same global irradiance (almost 1700 kWh/m^2) in the Southern of Italy have been considered: Napoli and Messina. Both these locations have high GHI, but they show a significant difference in the ratio between the Direct Normal Irradiance (DNI) and the diffuse irradiance. In the following Section the two plants configuration and control strategy are presented. Then the performance of each plant is firstly assessed for the two locations and secondly the results for the different technologies compared. The same heating and cooling temperatures required by the user are considered for both plants to fairly compare their energy performance.

3. Description of the plants

3.1. Plant 1

Apart from the size of the solar field, the plant has the same specifications as the real experimental system designed and tested by some of the authors in the STS National research project. In particular, it consists of: (i) a 146 m^2 Compound Parabolic Collector solar field produced by Kloben Sud [41]; (ii) a diathermic oil storage tank of 3 m^3; (iii) a 3.5 kW regenerative Organic Rankine Cycle unit manufactured by Newcomen; and (iv) a 17 kWc Yazaki Energy System [42] absorption chiller (Figure 1). As regards the solar field, the absorbing surface of the collectors is made of Al–N/Al selective material having an absorptance coefficient $\beta>0.92$ and an emittance coefficient $\varepsilon<0.065$. Copper tubes for high vacuum applications allow to achieve heat fluid temperatures up to 200°C. A diathermic oil storage tank using therminol 62 as thermal vector [43] is used to decouple solar field and ORC unit.

The ORC unit operates according to a regenerative cycle using R245fa as working fluid. The related expander is a three radial cylinders alternative engine. The thermal power output from the ORC unit is recovered for heating and cooling purposes depending on seasonality. In the hot season, the rejected heat is directed to the absorption chiller to provide cold water to the user at nominal temperatures of about 7°C. In terms of performance, the absorption chiller has a nearly 0.7 nominal coefficient of performance (COP) with an inlet hot water of 88°C. However, it is able to work with acceptable performance up to a minimum inlet water temperature of about 70°C, representing a good compromise for the operation of the overall system.

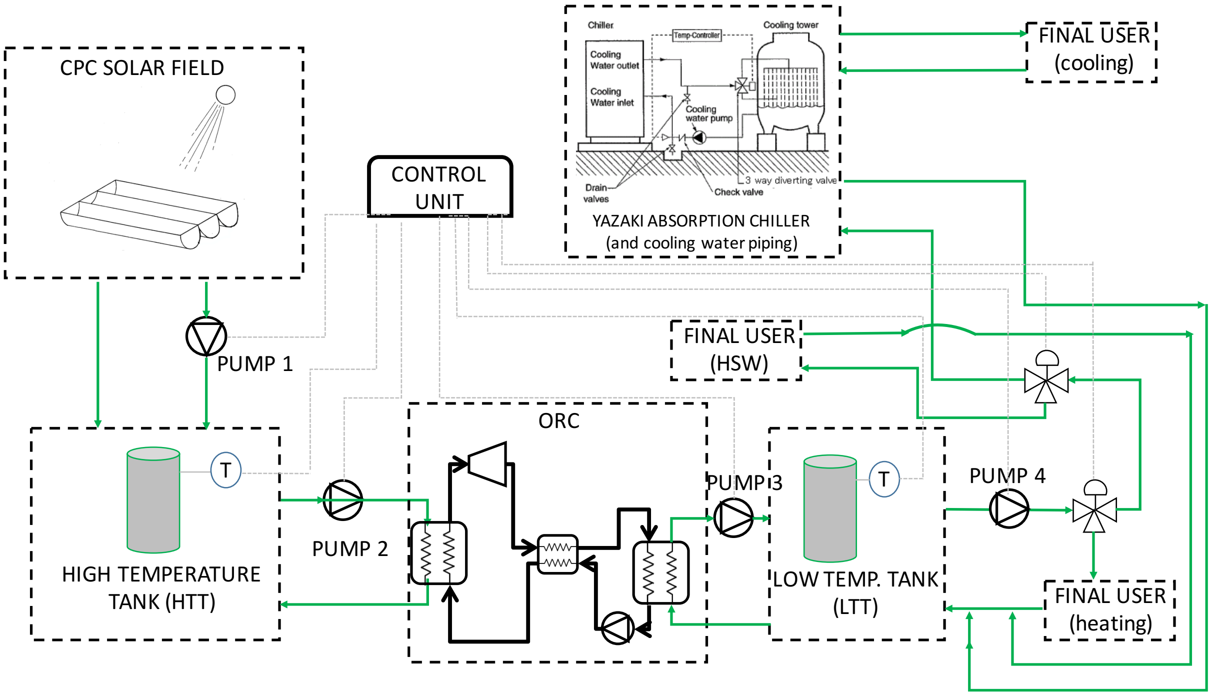

Fig. 1 - Functional scheme of Plant 1.

3.2. Plant 2

Plant 2, instead, is based on the innovative micro-Combined Heat and Power (m-CHP) plant, developed by the consortium of several Universities and industrial organizations under the EU funded Innova MicroSolar Project [37]. In this work a trigeneration configuration is assumed. Therefore, it consists of: (i) a 146 m^2 concentrated LFR solar field, with 240 m^2 gross encumbrance, producing heat at temperatures in the range 250-280 °C; (ii) a 3.2 kWe Organic Rankine Cycle plant; (iii) an advanced PCM thermal storage tank equipped with reversible heat pipes; and (iv) a 17.6 kWc absorption chiller (Figure 2).

The receiver consists of evacuated tube collectors placed at about 3.5 m from the ground and able to reach a maximum operating temperature of 400°C. At nominal operating conditions (DNI equal to 900 W/m^2) the peak thermal power output is about 80 kWt as declared by the manufacturing company [44].

The ORC unit designed by ENOGIA [45] operates accordingly to a regenerative cycle using NOVEC 649 as working fluid [46]. The thermal energy storage system, as designed by Northumbria University and Aavid Thermacore [47] and investigated by Lleida University [48], consists of 3.8 tons of nitrate solar salt kNO_3 (40wt. %)/$NaNO_3$ (60wt. %), whose melting temperature is in the range 216-223°C [49]. It has a heat storage capacity of about 100 kWh latent heat in order to guarantee 4 hours of ORC unit operation during night time with a nominal input power of 25 kW. Reversible heat pipes, as developed by Aavid Thermacore [47], are adopted to transfer heat both from the solar field to the storage tank and from the storage tank to the ORC unit, depending on the operating conditions. Based on the solar radiation and the state of charge of the TES the plant is able to switch from an operation mode to another according to the control system developed by S.TRA.TE.G.I.E. srl [50].

In addition, the 17.6 kWc Yazaki absorption chiller, as in the case of Plant 1, was considered to produce chilled water by recovering the thermal output power of the ORC unit in summer.

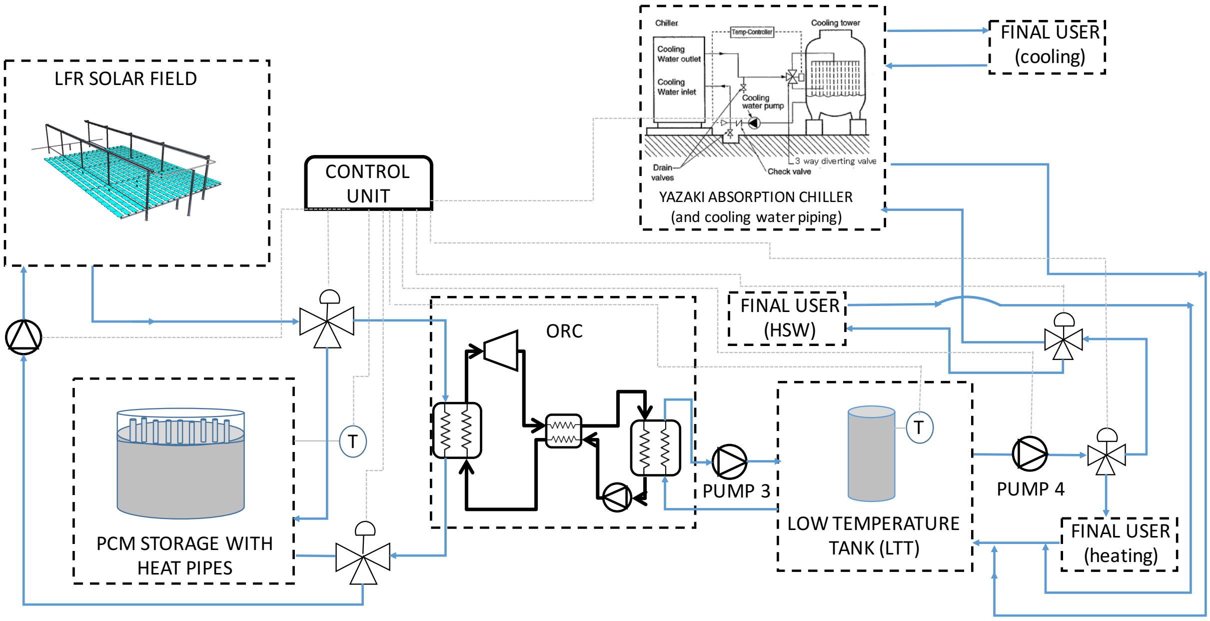

Fig. 2 - Functional scheme of the Plant 2.

4. Description of the models

The models of the two plants described above have been developed in TRNSYS [51]. Despite TRNSYS has many library built-in components, ad-hoc subroutines have been developed by the authors in Matlab [52] for modelling the main components. In this work, both plants operate to produce electricity, while the thermal load is considered a by-product which can be entirely collected and used for space heating, hot water or cooling depending on seasonality. According to the Italian decree 412/93 [32], which fixes the heating period for the different locations in Italy, the heating period corresponds to 15 November – 31 March in Napoli and 1 December – 31 March in Messina. The cooling period, instead, was assumed to be the same for both locations and it ranges from 1 June to 30 September. As regards the temperatures at the condenser, they have been fixed to satisfy the related heating and cooling needs, assuming radiant distribution systems in the supplied building with radiant panel floors, where the temperature on the return branch from heating system is set to 28°C and the temperature on the return branch from the cooling system is set to 15°C. The temperature of the heating water ranges from 28 to 33°C in the cold period. In the mid-season, when there is neither heating nor cooling demand, the energy from the LTT (Low Temperature Tank) is used to satisfy the domestic hot water demand and the inlet water is 50-55°C. In summer the temperature range is 70-75°C to supply adequate thermal power to the absorption chiller. The operation of the mixers and the diverters, as reported in Figures 1 and 2, depends on seasonality.
Further details are provided in the following sections.

4.1 Plant 1

As regards the model of Plant 1, it consists of the following main components: Type 71 for the CPC solar field; Type 4 for both the diathermic oil tank (HTT) and the hot water storage tank (LTT), Type 155 for calling the ORC subroutine developed in Matlab, Type 107 for the absorption chiller and Type 510 for the evaporative cooling tower.

According to the CPC model in TRNSYS, the useful thermal power from the solar field $P_{SF,out}$ is equal to:

$$P_{SF,out} = A \cdot (\eta_0 \cdot (G_b \cdot K_\theta + G_d \cdot K_d) - a_0 \cdot (T_m - T_a) - a_1 \cdot (T_m - T_a)^2) \quad (1)$$

where A is the collector area, G_b and G_d the direct and diffuse radiation on collector plane, K_θ and K_d the Incident Angle Modifier (IAM) for direct and diffuse radiation respectively, T_m the mean temperature of the fluid in the collector, T_a the ambient air temperature and η_0 the maximum optical efficiency. Finally, a_0 and a_1 are coefficients which depend on type and model of the collectors considered and are equal to 0.974 and 0.005 $W/m^2 \cdot K$ respectively in this case. With reference to the ORC unit, it has been modelled considering steady state conditions based on the following assumptions: (i) a minimum driving temperature difference between the evaporator and the condenser equal to 50°C; (ii) a minimum temperature difference of 34°C between the inlet diathermic oil and the evaporating temperature; (iii) an overheating of 5°C and a maximum evaporation temperature of 149°C (iv) a minimum pressure ratio at the expander of 2.5 and a maximum inlet pressure of 25 bar; and (v) an expander isentropic efficiency varying in the range 46-60% and an isentropic efficiency of the pump equal to 70%. Moreover, pressure drops and thermal capacity of the components have been neglected, whilst efficiency of the heat exchangers fixed constant. In particular, the evaporator has been modelled according to the ε-NTU method, while the exact characterization of the heat transfer coefficients in the different regions of the vapour generator neglected.
Hence, the electric power produced by the ORC is equal to:

$$P_{ORC,el} = \dot{m}_f \cdot [\eta_m \cdot \eta_{el} \cdot \Delta h_e - \Delta h_p / (\eta_m \cdot \eta_{el})] \quad (2)$$

where $\dot{m}_f$ is the organic fluid flow rate, η_m and η_{el} the mechanical and electric efficiencies assumed equal to 95% and 90% respectively, Δh_e and Δh_p the actual specific enthalpy difference across the expander and the pump.
With regard to the output thermal power, it is evaluated as in Eq. 3:

$$P_{ORC,out} = \dot{m}_c \cdot c_{p,c} \cdot (T_{out} - T_{in}) \quad (3)$$

with $\dot{m}_c$ the water flow rate, $c_{p,c}$ the specific heat of the water and T_{out} and T_{in} the outlet and inlet temperatures of the water at the condenser.
In particular, a minimum temperature difference between the inlet temperature of the cooling water and the condensing temperature of the working fluid has been fixed equal to 12°C.
The cooling power of the absorption chiller is equal to Eq. 4:

$$P_{abs} = P_{abs,in} \cdot COP \quad (4)$$

where $P_{abs,in}$ is the inlet thermal power and COP depends on the operating conditions.
Table 1 reports the operating conditions of Plant 1 where HTT_ΔT the working temperature ranges of the HTT storage. As shown in a previous work of the authors [36], this parameter is remarkable respect to the system optimization and it is requested for the proper system adjustment. The meaning of this temperature range is that when the temperature available at the HTT storage tank to the ORC feeding reaches the higher temperature of the range, the ORC unit switches on while when it goes down below the lower value of the range, the ORC unit switches off. Three optimal values of this temperature range have been fixed respectively for hot, cold and mid seasons. The mass flows reported in table 1 regards the pumps visible in Figure 1.

Table 1 Operating conditions of Plant 1

Operating conditions	Value
HTT_ΔT_h	170-160 °C
HTT_ΔT_c	120-110 °C
HTT_ΔT_m	160-135 °C
mass flow rate of PUMP1	7000 kg/h
mass flow rate of PUMP2	1800 kg/h
mass flow rate of PUMP3	3600 kg/h
mass flow rate of PUMP4	4320 kg/h
Cooling water pump	9180 kg/h

4.2 Plant 2

With respect to Plant 2, the following main components have been included into the model: (i) the LFR solar field; (ii) the micro ORC plant; (iii) the PCM thermal energy storage tank equipped with reversible heat pipes; (iv) the absorption chiller. In this case, specific subroutines for the LFR solar field and the PCM storage tank equipped with heat pipes have been developed by the authors in Matlab in addition to that of the ORC unit. As for the model of Plant 1, Type 107 and Type 510 have been used to model the absorption chiller and the evaporative cooling tower. Finally, mixers and diverters as in Figure 3 are included into the model to divert the flow of the oil according to the operation mode of the plant.

The performance of the LFR solar field has been assessed in terms of its optical efficiency under quasi-steady state conditions. The maximum optical efficiency of the LFR is reached when the incident angle is zero and can be expressed as in Eq. 5:

$$\eta_{opt} = \eta_{opt,max}(\theta = 0) \cdot IAM(\alpha, \sigma) \tag{5}$$

where θ is the solar incident angle, α the solar elevation and σ and the azimuthal angle. The values of IAM for the considered collector have been provided by the manufacturing company ELIANTO [8] at different solar elevation and azimuthal angles.

Therefore, taking into account the thermal losses of the absorber tubes Q_{loss} the collected thermal energy of the LFR can be calculated as in Eq. 6:

$$P_{SF,out} = A \cdot DNI \cdot cos(\theta) \cdot \eta_{opt} \cdot \eta_{rec} - Q_{loss} \tag{6}$$

where, A is the area of the primary collectors, cos(θ) the cosine of the solar incident angle and η_{rec} the receiver efficiency

The oil flow rate in the solar field is adjusted in order to keep the oil temperature at 210°C when the solar field supplies the ORC, thus assuring a good electric conversion efficiency of the ORC unit or at 10°C more than the average TES temperature in case the solar field supplies the storage.

The model of the ORC unit is similar to that of Plant 1 considering: (i) a constant temperature difference between the inlet oil from the plant (LFR and or TES) and the evaporating temperature of the working fluid equal to 34°C if the cycle is subcritical (otherwise the evaporating temperature is set 5°C lower than the critical temperature); (ii) a minimum superheating of 5°C at the evaporator outlet; (iii) no subcooling at the condenser; and (iv) pump and turbine isentropic efficiencies varying with operating conditions according to the data provided by the manufacturing company ENOGIA [45].

The PCM storage tank has been modelled according to the guidelines of the IEA Task 32 report on advanced storage concepts [53], where a detailed description of Type 185 is provided. The model is based on the following main assumptions: (i) material isotropic and isothermal in each

internal time-step; (ii) no hysteresis and subcooling effects; and (iii) charging and discharging not simultaneous. The presence of heat pipes is modelled by both limiting the maximum power exchanged to 40 kW and fixing a minimum temperature difference between the oil and the PCM equal to 5°C.
Hence, the temperature variation of the PCM due to the heat exchanged is given by:

$$\Delta T_{PCM(t+1)} = \Delta T_{PCM(t)} \cdot e^{-[\Delta t_{int-timestep} \cdot k]} \quad (7)$$

where k is a function of both PCM and oil thermal properties [53]. Then, from the temperature variation of the PCM, it is possible to calculate the heat exchanged as:

$$Q_{PCM(t+1)} = \int_t^{t+1} Q_{PCM(t)} \cdot dt \quad (8)$$

The model of the absorption chiller is the same as in Plant 1.
The operation mode of the plant depends on the solar radiation and the state of charge of the TES. The diathermic oil from the solar field flows to the TES and/or directly to the ORC depending on its temperature and on the amount of power collected at the receiver. On the contrary, when the power produced by the solar field is low or zero and the average TES temperature is within a given operating range ($T_{ORC,on}$=217°C and $T_{ORC,off}$=215°C), the thermal energy of the TES can be used to run the ORC unit and assure its operation for a maximum of 4 hours with no sun. Table 2 reports set-points and threshold values of each operation mode (OM), while Figure 5 shows the control logic flow chart of Plant 2.

Table 2 Operating conditions for the different operation modes of Plant 2

Operation Mode	Description	Operating conditions
OM1	LFR supplies ORC	T_{oil}=210°C
OM2	System off	-
OM3	LFR supplies TES	T_{oil}=$T_{TES,av}$+10°C
OM4	LFR supplies TES and ORC	T_{oil}=210°C if $T_{TES,av}$<200°C or $T_{TES,av}$>280°C otherwise T_{oil}= $T_{TES,av}$ +10°C if $T_{TES,av}$ >200°C
OM5	TES supplies ORC	oil flow rate 0.22 kg/s
OM6	TES and LFR supply ORC	T_{oil}=210°C and oil flow rate 0.22 kg/s

Further details of the ad-hoc subroutines can be found in [40].

5. Results and discussion

In order to evaluate the influence of the incident solar radiation on the performance of the integrated systems, both plants have been investigated for two different Italian locations. These locations exhibit an annual global irradiance of almost 1700 kWh/m^2, that is a significant amount for the effective operation of solar heat and power systems. In particular, the following locations have been considered: (i) Napoli (local coordinates 40° 85′ 17.75″ N and 14° 26′ 81.24″ E), which has a global irradiance of about 1682 kWh/m^2 and a ratio of DNI to diffuse irradiance R_{irr} of 1.478, and (ii) Messina (local coordinates 38° 19′ 38.14″ N and 15° 55′ 40.15″ E), which despite a similar global irradiance, namely 1695 kWh/m^2, has a value of R_{irr} of about 2.4816. Weather data have been taken from Meteonorm database on an hourly basis, while the simulation time step fixed to 10 minutes.
Firstly, the performance of the plants has been evaluated in terms of energy production on a monthly basis. Independently from the location, the energy produced by the solar field is much

higher during summer and mid-season than in winter time, because of the higher solar irradiance and hours of irradiation.

Furthermore the following conversion efficiencies have been assessed: (i) the solar field efficiency (η_{SF}), defined as the ratio between the output power from the solar collector and the input solar power ; (ii) the electric efficiency of the ORC ($\eta_{ORC,el}$), defined as the ratio between the output electric power and the inlet thermal power to the ORC; (iii) the thermal efficiency of the ORC ($\eta_{ORC,th}$), defined as the ratio between the output and input thermal power of the ORC; (iv) the thermal energy storage efficiency (η_{TES}), defined as the ratio between the outlet thermal energy towards the ORC (discharging) and the inlet thermal energy from the solar field during its charging; and finally (v) the coefficient of performance (COP), i.e. the ratio between the cooling power and the input thermal power of the absorption chiller.

5.1 Plant 1

Results for Plant 1 have been represented in Figures 3a and 3b. As expected the output energy from the solar field is much lower than the input solar radiation, while it is equal to the input energy to the TES, because of the plant configuration.

As regards the energy production, the electricity produced is adequate to satisfy the request of a residential dwelling with 5 occupants [54] of approximately 4100 kWh_e considering that in the case of our plants the quota of energy due to the cooling load is satisfied by the absorption chiller of the CCHP system. The highest electric energy production is achieved in the mid-season, because of the higher temperature difference between the HTT and the LTT. On the contrary, the highest thermal energy output from the ORC unit is obtained in the hot season, thus positively contributing to the cooling production.

From the analysis of the results, it is evident that the performance of Plant 1 is not significantly affected by the considered location. More precisely, the conversion efficiency of the solar field is weakly influenced by location in case of CPC technology. Indeed, the mean annual conversion efficiency of the solar field is the same (36.2%).

Even the conversion efficiency and the operating hours of the ORC unit are more or less the same in the two considered locations, proving that such system is not affected by the ratio of the DNI to the diffuse irradiance. For example, the electric efficiency ranges between 3.0 and 7.4 % in Napoli and between 3.0 and 7.1 % in Messina.

The performance of the plant has been also analysed on an hourly basis for typical working days in winter and summer as reported in Figures 4a-d. The collected thermal energy from the solar field during the typical winter day is enough to supply the ORC unit almost at its nominal operating conditions (Figure 4a and 4c). Moreover, considering the trend in Napoli of Figure 4, it is evident that even low thermal input and output power from the solar field are beneficial for the operation of the plant. Indeed, in the period 1 pm – 2 pm, when the solar radiation is low, the TES discharges energy to the ORC unit, whilst at a certain time after 2 pm the ORC is switched off and the TES is charged. Therefore the TES helps to balance the system, reducing the effect of solar irradiance variation. Despite the solar irradiance higher than irradiance of wintertime, the ORC unit is prone to frequent on-off in summer season in Napoli. On the other hand, in Messina the solar radiation is higher compared to Napoli for both the typical winter and summer day and, as a consequence, less interruptions occur, thus extending the operation and the reliability of the system. However the electrical and thermal output power of the ORC in Messina and Napoli are similar. Finally, because of the LTT, the absorption chiller has a lower tendency to interruptions compared to the ORC unit in both locations.

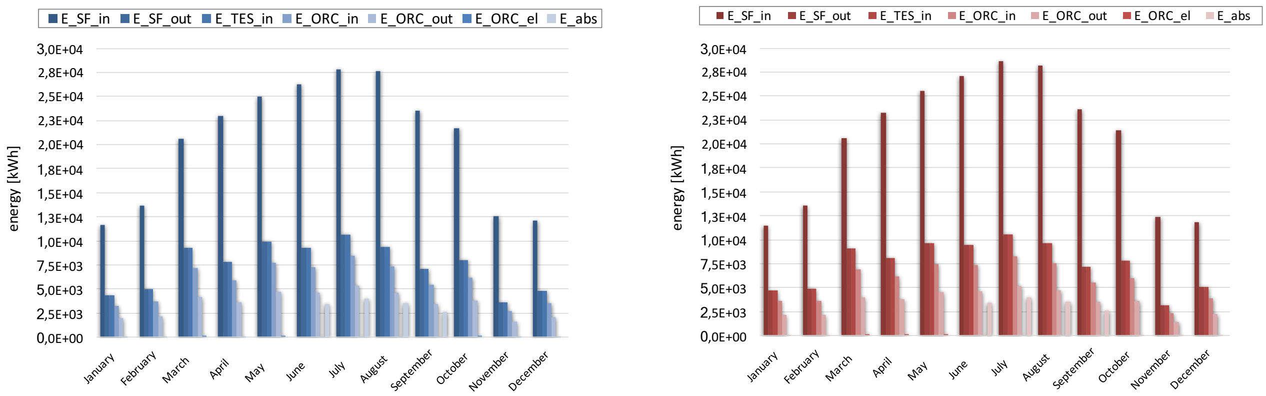

(a) (b)

Fig. 3 - Monthly energy balance of <u>Plant 1</u>: a) in Napoli; b) in Messina.

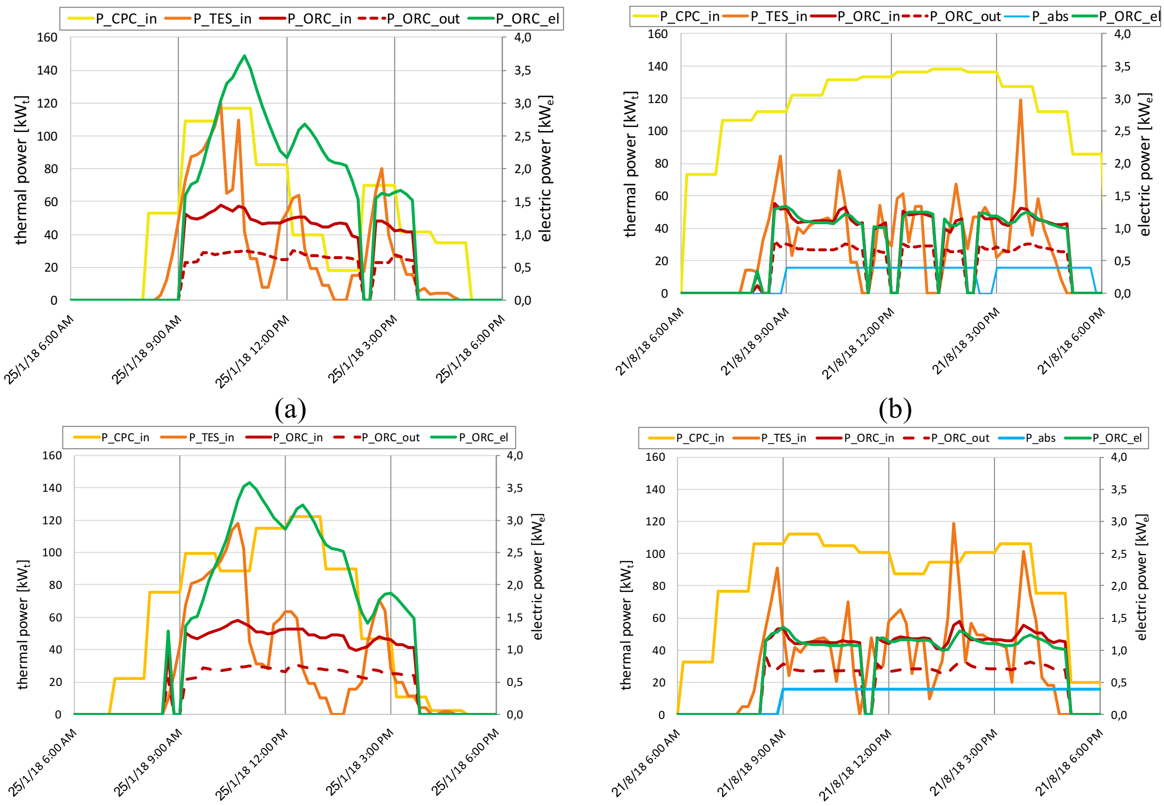

(a) (b)

(c) (d)

Fig. 4 - Daily trend of performance of Plant 1 for typical days in (a) winter in Napoli, (b) summer in Napoli, (c) winter in Messina, (d) summer in Messina

5.2 Plant 2

Figures 5a-b represent the results obtained for Plant 2. Because of the plant configuration and operating strategy, the output thermal energy from the solar field goes mostly to the ORC unit and only a reduced amount is directed to the TES.

The conversion efficiency and the operating hours of the system significantly change with location as reported in Tables 5 and 6, thus proving that such system is affected by the ratio of the DNI to the diffuse irradiance. Indeed, its performance are significantly higher in Messina rather than in the city of Napoli.

In particular, due to the higher R_{irr} in Messina: (i) the mean annual conversion efficiency of the solar field is about 2.7% higher than in Napoli; (ii) the ORC unit works around 500 operating hours more; (iii) the electrical and thermal energy production of the ORC unit are about 19% higher; and (iv) the operating hours of the absorption chiller are almost 15% higher.

As regards the TES, because of the plant operation mode, the mean annual efficiency is significantly lower compared to that of Plant 1. In winter, indeed, the TES temperature remains often below the melting point and, as a consequence, the stored energy is not usefully exploited. The performance of Plant 2 strictly depends on the operation modes (discussed in Section 4.2) which in turn are related to the solar radiation and state of charge of the TES. More precisely: in OM1 the LFR supplies the ORC only, in OM4 the LFR supplies both the TES and the ORC , in OM5 the TES supplies the ORC, while in OM6 both the TES and the LFR supply the ORC. In Table 3 the performance of the plant is reported with respect to the operation modes for the city of Messina.

Table 3 - Performance data of ORC unit for Plant 2 with different operation modes in the city of Messina

		Jan	Feb	Mar	Apr	May	Jun	Jul	Aug	Sep	Oct	Nov	Dec	Working hours
OM4	$P_{ORC,in}$ [kW]	24.7	24.8	24.9	24.7	24.8	24.6	24.6	24.6	24.5	24.7	24.0	24.6	2147 h
	$P_{ORC,out}$ [kW]	18.5	18.9	19.2	19.7	19.9	20.5	20.7	20.6	20.4	19.6	18.6	18.3	
	$P_{ORC,el}$ [kW]	3.02	3.12	3.18	2.57	2.61	1.80	1.83	1.81	1.78	2.50	2.35	2.97	
	$Eff_{ORC,el}$ [%]	11.1	11.1	11.4	9.3	9.4	6.5	6.6	6.5	6.5	9.1	8.8	11.0	
OM5	$P_{ORC,in}$ [kW]	18.8	18.3	18.5	16.8	16.9	15.1	15.1	15.1	15.0	16.5	16.6	0.0	801 h
	$P_{ORC,out}$ [kW]	13.9	13.6	13.7	12.9	13.0	12.2	12.2	12.1	12.1	12.7	12.8	0.0	
	$P_{ORC,el}$ [kW]	1.85	1.75	1.77	1.08	1.11	0.38	0.39	0.37	0.36	0.98	1.04	0.0	
	$Eff_{ORC,el}$ [%]	9.5	9.2	9.2	6.2	6.3	2.4	2.4	2.4	2.3	5.7	6.0	0.0	
OM6	$P_{ORC,in}$ [kW]	0.00	22.77	21.90	20.63	21.90	18.97	19.09	20.08	19.39	21.06	21.04	0.0	225 h
	$P_{ORC,out}$ [kW]	0.00	16.81	16.19	15.72	16.70	14.99	15.13	15.87	15.30	16.06	15.99	0.0	
	$P_{ORC,el}$ [kW]	0.00	2.67	2.46	1.81	2.01	1.02	1.02	1.16	1.09	1.85	1.86	0.0	
	$Eff_{ORC,el}$ [%]	0.0	11.0	10.5	8.2	8.6	4.8	4.8	5.2	5.1	8.1	8.3	0.0	

In Table 3, the performance of the Plant in OM1 has been omitted, since this operation mode is limited to about 88 h/year and it occurs in between the other operating modes (e.g. before OM4, when the solar power is so high to supply not only the ORC, but even the TES). Consequently, the thermal energy input to the TES is very low and the electric energy and efficiency close to zero. From the analysis of the results reported in Table 3 it is evident that Plant 2 operates mostly on mode OM4 (2147 h), achieving a maximum monthly mean electric efficiency of the ORC of about 11.4% in March. Because of the different condensing temperatures during the year the monthly mean electric output power in OM4 ranges from 1.78 kWe in September to 3.18 kWe in March. On the contrary, the thermal output power is almost constant throughout the year and achieves its maximum in July. Because of the set-point temperatures of the TES, the ORC is able to achieve high conversion efficiencies also in mode OM6, when both the LFR and the TES supply thermal power to the ORC. However, this operating mode is limited to about 225 h/year and it does not occur in January and December, due to the limited excess solar radiation for charging also the TES. Also OM5, which reaches 801 hours of operation annually, does not occur in December and it is mainly present in summer season.

Figures 6a-d, instead, report the daily performance trend. Despite a power input in the range 80-120 kWt during the morning of the considered winter day in Napoli (Figure 6a), the daily performance is limited. Indeed, as subsequently shown in Figure 7a, the temperature of the TES is too low to run the ORC unit and, as soon as the input power to the solar field goes down at noon, the ORC unit is switched off. On the contrary, for the city of Messina, thanks to the constant thermal power input throughout the considered winter day, the produced energy is higher and a small amount of energy is also supplied to the TES for its charging. Independently from the location, in summer, Plant 2 exhibits very good performance especially because generates electric and cooling power uninterruptedly, as evident in Figures 9b and 9d. The prolonged radiation indeed allows to simultaneously run the ORC unit and charge the TES, thus extending the operation of the ORC and the power production also after sunset. However, because of the higher condensing temperatures compared to the winter season, the electric power output remains below 2 kWe. As regards the absorption chiller, its operation is prolonged also during night, thanks to the temperatures achieved in the LTT. The thermal output power of the ORC, indeed, is directed to the LTT and once its temperature is above the threshold value, the absorption chiller switches on.

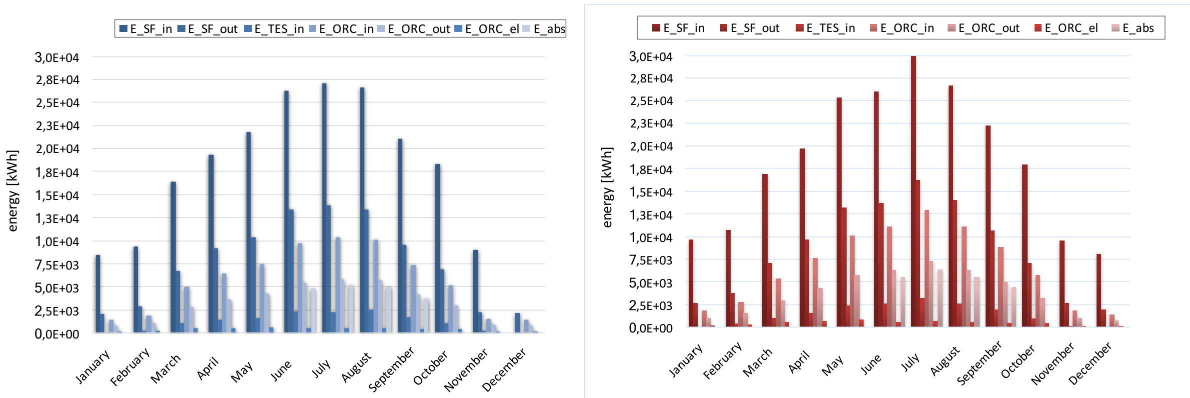

Fig. 5 - Monthly energy balance of Plant 2: a) in Napoli b) in Messina

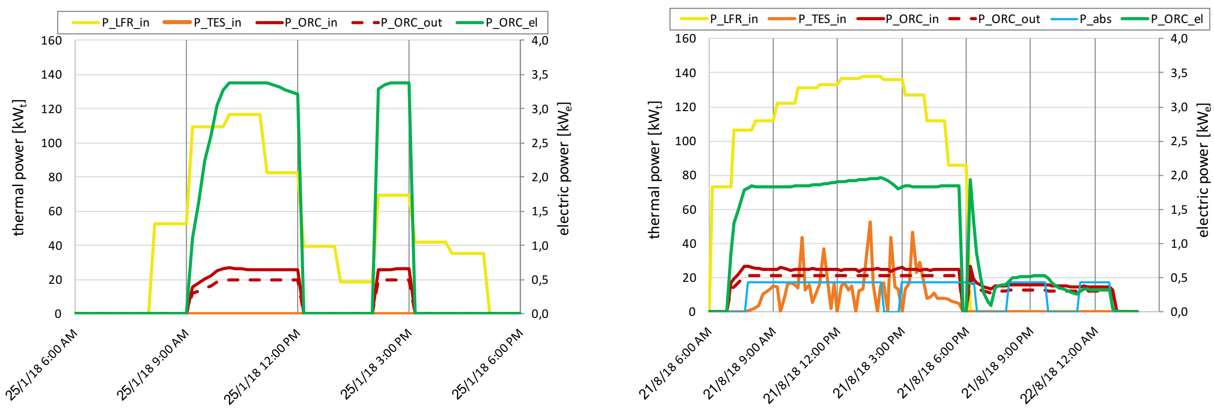

(a) (b)

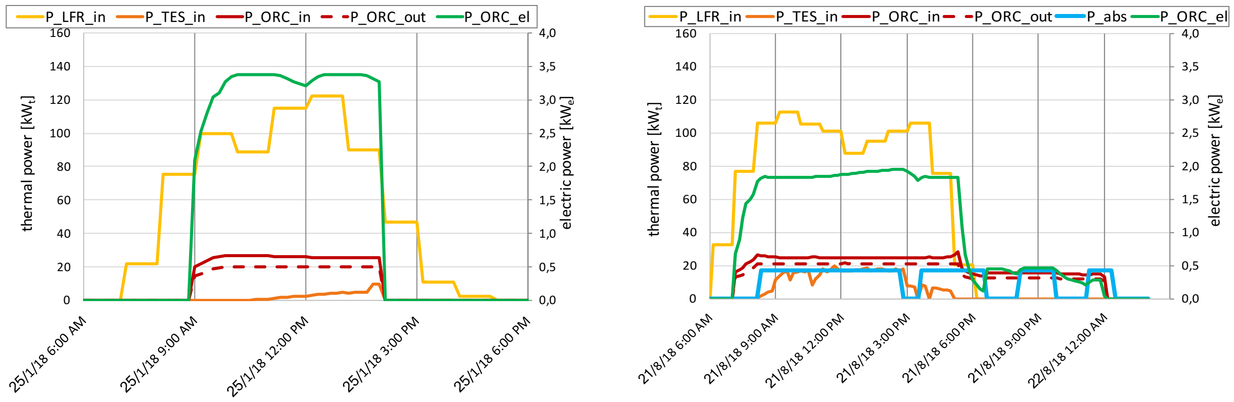

(c) (d)

Fig. 6 - Daily trend of performance of Plant 2 for typical days in (a) winter in Napoli, (b) summer in Napoli, (c) winter in Messina, (d) summer in Messina

5.3 Comparative analysis of the two plants

Finally, the monthly performance of the two plants has been compared with the final aim to achieve a thoughtful understanding of their operation. In general, in the period October-April the output energy from the ORC unit is higher for Plant 1. On the contrary, in summer, independently from the location, the output energy is higher for Plant 2 and, as a consequence, also the cooling energy produced. Tables 4 and 5 report the mean monthly conversion efficiencies and energy output of Plant 1 for the city of Napoli and Messina while Tables 6 and 7 those of Plant 2.

Although the higher irradiance and number of operating hours of the system during the hot season, for every plant the electric efficiencies of the ORC are lower in summer because of the higher condensation temperature necessary to run the absorption chiller. In particular, they are less than half of the electric efficiency achieved in winter time. This minor performance of the ORC unit is compensated by the cooling effect obtained by means of the absorption chiller. More in detail, Plant 2 is much more affected by seasonality compared to Plant 1. Indeed, the conversion efficiency of the solar field ranges from 22.9% in December to 51.1% in June for the city of Napoli and from 27.6% in January to 54.2% in July for Messina. The ratio between the maximum and the minimum mean monthly conversion efficiency is about 2.23 for the LFR solar field, whilst it is about 1.72 for the CPC.

Because of the higher operating temperatures of the PCM storage tank of Plant 2 compared to the HTT of Plant 1, the electric efficiency of the ORC ($\eta_{ORC,el}$) unit is significantly higher for the former and it achieves a mean value of 11.3% in December in Messina. In addition, Plant 2 is able to achieve a higher electrical production than Plant 1, independently from the location. In particular, it is almost 75% higher in the case of Messina. Also the thermal energy production is higher than that of Plant 1 in Messina, whilst it is lower in Napoli. Because of the substantially higher conversion efficiency of the solar field in summer, the thermal energy production and the related cooling energy is higher for Plant 2 during this season. As a consequence, the cooling energy production of Plant 2 is significantly higher and around 58.5% more than that of Plant 1 for the city of Messina. Therefore, in case of high DNI, LFR technology performs much better than CPC, resulting especially suitable for solar cooling applications.

Table 4 Monthly performance of Plant 1 for the city of Napoli

Month	η_{SF} [%]	$\eta_{ORC,el}$ [%]	$\eta_{ORC,th}$ [%]	η_{TES} [%]	h_{ORC}	$E_{ORC,el}$ [kWh]	$E_{ORC,out}$ [kWh]	COP	h_{abs}	E_{abs} [kWh]
Jan	36.8%	6.1%	73.5%	100.0%*	92.0	196.1	2381.7	-	-	-
Feb	36.3%	5.9%	73.5%	98.2%	104.3	217.3	2687.0	-	-	-
Mar	45.1%	7.4%	71.1%	99.3%	181.8	534.4	5108.7	-	-	-
Apr	33.8%	5.4%	75.1%	97.8%	157.7	318.8	4421.2	-	-	-
May	39.8%	5.8%	74.5%	99.2%	191.3	447.8	5782.3	-	-	-
Jun	35.4%	3.0%	77.9%	97.9%	182.2	215.4	5647.3	0.65	214.0	3407.3
Jul	38.0%	3.0%	78.1%	99.2%	206.0	246.4	6566.0	0.64	252.6	4011.2
Aug	33.9%	3.0%	77.6%	99.1%	195.5	223.1	5717.3	0.64	220.2	3497.1
Sep	30.0%	3.1%	77.8%	98.0%	147.8	167.0	4259.6	0.65	163.7	2605.0
Oct	36.8%	5.6%	75.0%	99.6%	161.7	345.1	4641.1	-	-	-
Nov	28.6%	5.6%	74.6%	98.3%	75.3	150.2	2004.2	-	-	-
Dec	39.9%	6.4%	72.9%	97.8%	98.3	226.8	2595.9	-	-	-
Total	**36.2%**	**5.0%**	**75.1%**	**98.7%**	**1794.0**	**3288.5**	**51812.6**	**0.65**	**851.8**	**13520.6**

*because of initialization

Table 5 Monthly performance of Plant 1 for the city of Messina

Month	η_{SF} [%]	$\eta_{ORC,el}$ [%]	$\eta_{ORC,th}$ [%]	η_{TES} [%]	h_{ORC} [h]	$E_{ORC,el}$ [kWh]	$E_{ORC,out}$ [kWh]	COP	h_{abs} [h]	E_{abs} [kWh]
Jan	40.9%	6.4%	72.5%	100.0%*	98.2	229.5	2600.0	-	-	-
Feb	36.0%	6.0%	72.6%	98.2%	102.5	218.8	2636.6	-	-	-
Mar	44.1%	7.1%	71.8%	98.4%	179.5	491.7	4945.1	-	-	-
Apr	34.6%	5.6%	75.1%	98.8%	162.2	345.2	4647.0	-	-	-
May	37.7%	5.6%	74.7%	99.2%	192.7	419.2	5596.2	-	-	-
Jun	34.7%	3.0%	77.8%	98.3%	188.7	218.3	5716.3	0.65	216.7	3451.3
Jul	36.7%	3.0%	77.8%	99.0%	211.3	243.9	6426.7	0.64	247.9	3936.3
Aug	34.0%	3.1%	77.6%	99.1%	198.7	229.8	5841.8	0.64	224.5	3564.4
Sep	30.2%	3.0%	77.8%	98.7%	147.8	169.5	4328.4	0.65	164.1	2609.7
Oct	36.3%	5.5%	74.9%	98.9%	158.8	327.5	4498.3	-	-	-
Nov	25.5%	5.5%	75.1%	94.9%	61.7	127.2	1743.5	-	-	-
Dec	43.1%	6.4%	72.1%	99.3%	105.0	248.9	2784.3	-	-	-
Total	**36.2%**	**5.0%**	**75.0%**	**98.6%**	**1807.0**	**3269.6**	**51764.1**	**0.65**	**853.2**	**13561.7**

*because of initialization

Table 6 Monthly performance of Plant 2 for the city of Napoli

Month	η_{SF} [%]	$\eta_{ORC,el}$ [%]	$\eta_{ORC,th}$ [%]	η_{TES} [%]	h_{ORC} [h]	$E_{ORC,el}$ [kWh]	$E_{ORC,out}$ [kWh]	COP	h_{abs} [h]	E_{abs} [kWh]
Jan	24.3%	11.1%	69.1%	100.0%*	55.2	162.2	1010.6	-	-	-
Feb	30.6%	11.1%	69.1%	60.8%	72.3	211.9	1317.0	-	-	-
Mar	40.7%	11.1%	69.1%	82.3%	192.5	550.4	3440.6	-	-	-
Apr	47.5%	8.5%	70.0%	79.2%	250.5	546.6	4485.8	-	-	-
May	47.5%	8.5%	70.0%	79.4%	290.2	634.0	5213.0	-	-	-
Jun	51.1%	5.2%	69.4%	83.0%	376.8	508.1	6740.6	0.71	278.5	4789.3
Jul	51.0%	5.3%	69.6%	81.9%	398.5	548.9	7191.8	0.71	300.8	5173.3
Aug	50.1%	5.2%	69.3%	85.2%	396.0	525.8	7005.1	0.71	287.8	4949.8
Sep	45.4%	5.3%	69.9%	83.4%	285.8	385.5	5121.9	0.71	213.0	3663.0

Oct	37.6%	8.5%	70.0%	78.2%	202.8	441.4	3633.2	-	-	-
Nov	24.5%	9.1%	69.5%	73.2%	58.7	139.0	1058.9	-	-	-
Dec	22.9%	11.0%	69.1%	87.0%	52.7	154.0	963.4	-	-	-
Total	**39.4%**	**8.3%**	**69.5%**	**81.3%**	**2632.0**	**4807.9**	**47182.1**	**0.71**	**1080.1**	**18575.4**

*because of initialization

Table 7 Monthly performance of Plant 2 for the city of Messina

Month	η_{SF} [%]	$\eta_{ORC,el}$ [%]	$\eta_{ORC,th}$ [%]	η_{TES} [%]	h_{ORC} [h]	$E_{ORC,el}$ [kWh]	$E_{ORC,out}$ [kWh]	COP	h_{abs} [h]	E_{abs} [kWh]
Jan	27.6%	11.2%	69.2%	70.2%	68.8	207.9	1282.4	-	-	-
Feb	35.5%	11.1%	69.0%	68.3%	106.7	315.0	1950.5	-	-	-
Mar	42.2%	11.0%	69.1%	82.6%	205.8	588.5	3698.7	-	-	-
Apr	48.9%	8.5%	70.0%	81.3%	299.2	653.8	5363.4	-	-	-
May	52.0%	8.5%	69.9%	83.1%	399.2	858.2	7087.9	-	-	-
Jun	52.5%	5.2%	69.6%	83.5%	431.2	579.5	7691.7	0.71	319.0	5486.1
Jul	54.2%	5.1%	69.1%	86.4%	504.5	664.5	8929.7	0.71	369.6	6357.0
Aug	52.7%	5.2%	69.3%	87.1%	431.5	575.0	7685.0	0.71	321.5	5528.8
Sep	48.1%	5.3%	69.8%	82.1%	344.7	468.3	6181.3	0.71	258.0	4436.7
Oct	39.5%	8.5%	70.1%	78.3%	220.0	481.3	3985.8	-	-	-
Nov	27.9%	8.7%	70.5%	62.5%	72.8	164.9	1334.4	-	-	-
Dec	27.6%	11.3%	69.3%	6.5%	51.7	158.0	971.5	-	-	-
Total	**42.1%**	**8.3%**	**69.6%**	**72.7%**	**3136.0**	**5714.9**	**56162.2**	**0.71**	**1268.1**	**21808.7**

Finally, Figures 7 a-d show the daily trend of ORC electric efficiency together with the oil inlet temperature at the ORC evaporator and the average temperature of the storage tank for the typical winter and summer days in Napoli and Messina for both plants. Because of the lower concentration ratio of the CPC compared to the LFR, the inlet oil temperatures at the ORC unit and those of the storage tank are significantly lower in case of Plant 1. In Napoli, as anticipated, also during the winter day, the collected energy from the CPC solar field allows to achieve adequate temperatures at the HTT to run the ORC unit almost continuously in the period 9 am - 3 pm. On the contrary, despite the higher solar radiation during the summer day, Plant 1 has a tendency to frequent interruptions, because of the limited operating temperature range at the HTT and the higher condensing temperature, which does not allow to maintain always the minimum design temperature difference between the evaporator and the condenser of the ORC at 50°C. In case of Plant 2 in Napoli, the collected thermal energy allows to achieve the nominal ORC inlet temperature in short time also during the winter day. However, the collected thermal energy is not enough to charge the PCM up to its melting temperature and thus most part of this energy is then lost. Moreover, because of the low thermal input power to the solar field after noon, the ORC unit is switched off also during the day as previously discussed. During the summer day, instead, the collected thermal energy from the LFR is so high that it allows to achieve high oil temperatures at the inlet of the ORC and melt the PCM at the same time as reported in Figure 7b.
Similar trends occur in Messina. However, in this case Plant 1 exhibits limited shutdown during the summer day and Plant 2 runs without interruptions in the period 9 am - 2 pm also during the typical winter day because of the different profile of solar irradiance.

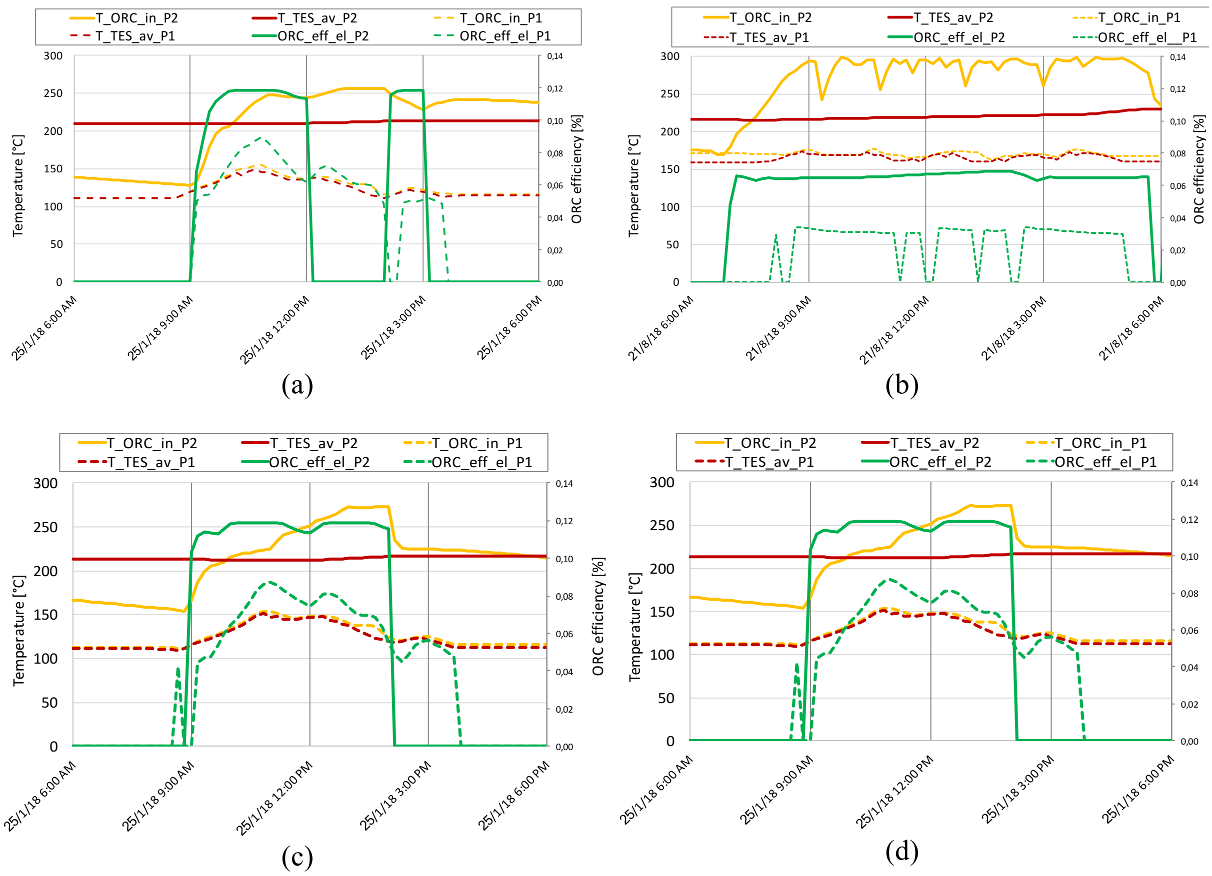

Fig. 7 - Daily trend of ORC electric efficiency with temperatures for Plant 1 and Plant 2 in (a) winter in Napoli, (b) summer in Napoli, (c) winter in Messina, (d) summer in Messina

6. Conclusions

In this work two different innovative solar ORC plants for trigeneration applications in the residential sector have been investigated by means of a numerical analysis in TRNSYS. Specific subroutines have been developed in Matlab by the authors to model the main components in more detail.

The dynamic performance of the considered systems has been evaluated with respect to two Italian locations distinguished by different radiation conditions. The comparison, that for the first time regards a complete in-depth analysis of two solar trigeneration systems powered by different CSP technologies, has brought to draw some interesting conclusions about the potential of different trigenerative system.

In general, the investigation has revealed the great influence of solar radiation on the effectiveness of such systems even for locations at similar latitudes. In particular, the main findings are summarized below:

- the LFR-ORC system shows an energy performance very sensitive to location. In Messina, indeed, the electrical and thermal energy production of the ORC unit when powered by LFR is about 19% greater than in Napoli. Furthermore, Plant 2 exhibits significant changes in energy production during the year and then seasonality has a considerable impact on this trend;
- the CPC-ORC is able to guarantee an electric and thermal energy output more constant throughout the year and less dependent on the quality of radiation, even if energy production is lower than Plant 2 for both locations. Moreover, in summer,

when the condensing temperatures are higher due to the absorption chiller, the electrical efficiency of the CPC-ORC is considerably limited;

- the LFR-ORC plant is able to achieve higher electric energy production despite the lower size of the ORC. Furthermore, in summer the LFR technology achieves higher conversion efficiencies that allow to obtain a significant thermal output from the ORC unit. As a consequence, in case of high DNI, LFR technology performs much better than CPC and thus results especially suitable for solar cooling applications

In conclusion, this study has highlighted the importance of proper design and technology selection with different radiation conditions, thus serving as a general guide for the adoption of similar technologies for trigeneration purposes at residential level.

Acknowledgements

This study is a part of the Innova MicroSolar Project, funded in the framework of the European Union's Horizon 2020 Research and Innovation Programme (grant agreement No 723596).
The research was partially supported by MIUR (Italian MInistry for education, University and Research), Law 232/2016, "Department of excellence".
We wish to thank also the company Enertecna for the prosecution of R&D activity of research project *STS – Solar Trigeneration System* from which started this activity regarding optimization of solar CCHP.

REFERENCES

[1] European Commission. Energy consumption in households - Eurostat Statistics Explained of European Commission 2018. https://ec.europa.eu/eurostat/statistics-explained/index.php/Energy_consumption_in_households (accessed September 3, 2018).

[2] Carrilho da Graça G, Augusto A, Lerer MM. Solar powered net zero energy houses for southern Europe: Feasibility study. Sol Energy 2012;86:634–46. doi:10.1016/j.solener.2011.11.008.

[3] Pietzcker RC, Stetter D, Manger S, Luderer G. Using the sun to decarbonize the power sector: The economic potential of photovoltaics and concentrating solar power. Appl Energy 2014;135:704–20. doi:10.1016/j.apenergy.2014.08.011.

[4] IEA. World Energy Outlook 2016. 2016.

[5] Viebahn P, Lechon Y, Trieb F. The potential role of concentrated solar power (CSP) in Africa and Europe—A dynamic assessment of technology development, cost development and life cycle inventories until 2050. Energy Policy 2011;39:4420–30. doi:10.1016/J.ENPOL.2010.09.026.

[6] desertec n.d.

[7] Hess D. The value of a dispatchable concentrating solar power transfer from Middle East and North Africa to Europe via point-to-point high voltage direct current lines. Appl Energy 2018;221:605–45. doi:10.1016/j.apenergy.2018.03.159.

[8] Chen GQ, Wu XF. Energy overview for globalized world economy: Source, supply chain and sink. Renew Sustain Energy Rev 2017;69:735–49. doi:10.1016/J.RSER.2016.11.151.

[9] Mathews JA. China's Electric Power: Results for first half 2017 demonstrate continuing green shift. vol. 15. 2017.

[10] INTERNATIONAL ENERGY AGENCY. World Energy Outlook 2017. 2017.

[11] IEA. Technology Roadmap Solar Thermal Electricity. 2014.

doi:10.1007/SpringerReference_7300.
[12] Watkins P, McKendry P. Assessment of waste derived gases as a renewable energy source – Part 2. Sustain Energy Technol Assessments 2015;10:114–24. doi:10.1016/j.seta.2015.03.004.
[13] Barlev D, Vidu R, Stroeve P. Innovation in concentrated solar power. Sol Energy Mater Sol Cells 2011;95:2703–25. doi:10.1016/j.solmat.2011.05.020.
[14] Jebasingh VK, Herbert GMMJ. A review of solar parabolic trough collector. Renew Sustain Energy Rev 2016;54:1085–91. doi:10.1016/j.rser.2015.10.043.
[15] Collado FJ, Guallar J. A review of optimized design layouts for solar power tower plants with campo code. Renew Sustain Energy Rev 2013;20:142–54. doi:10.1016/j.rser.2012.11.076.
[16] Shuai Y, Xia XL, Tan HP. Radiation performance of dish solar concentrator/cavity receiver systems. Sol Energy 2008;82:13–21. doi:10.1016/j.solener.2007.06.005.
[17] Zhu G, Wendelin T, Wagner MJ, Kutscher C. History, current state, and future of linear Fresnel concentrating solar collectors. Sol Energy 2014;103:639–52. doi:10.1016/j.solener.2013.05.021.
[18] Abbas R, Muñoz J, Martínez-Val JM. Steady-state thermal analysis of an innovative receiver for linear Fresnel reflectors. Appl Energy 2012;92:503–15. doi:10.1016/j.apenergy.2011.11.070.
[19] Santos-González I, García-Valladares O, Ortega N, Gómez VH. Numerical modeling and experimental analysis of the thermal performance of a Compound Parabolic Concentrator. Appl Therm Eng 2017;114:1152–60. doi:10.1016/j.applthermaleng.2016.10.100.
[20] Orosz M, Mueller A, Quoilin S, Hemond H. Small scale solar ORC system for distributed power 2009.
[21] Quoilin S, Broek M Van Den, Declaye S, Dewallef P, Lemort V. Techno-economic survey of organic rankine cycle (ORC) systems. Renew Sustain Energy Rev 2013;22:168–86. doi:10.1016/j.rser.2013.01.028.
[22] Cioccolanti L, Tascioni R, Arteconi A. Simulation analysis of an innovative micro-solar 2kWe Organic Rankine Cycle plant for residential applications. Energy Procedia, vol. 142, 2017, p. 1629–34. doi:10.1016/j.egypro.2017.12.541.
[23] Pei G, Li J, Ji J. Analysis of low temperature solar thermal electric generation using regenerative Organic Rankine Cycle. Appl Therm Eng 2010;30:998–1004. doi:10.1016/j.applthermaleng.2010.01.011.
[24] Wang J, Yan Z, Zhao P, Dai Y. Off-design performance analysis of a solar-powered organic Rankine cycle. Energy Convers Manag 2014;80:150–7. doi:10.1016/j.enconman.2014.01.032.
[25] Freeman J, Hellgardt K, Markides CN. Working fluid selection and electrical performance optimisation of a domestic solar-ORC combined heat and power system for year-round operation in the UK. Appl Energy 2017;186:291–303. doi:10.1016/j.apenergy.2016.04.041.
[26] Desai NB, Bandyopadhyay S. Thermo-economic analysis and selection of working fluid for solar organic Rankine cycle. Appl Therm Eng 2016;95:471–81. doi:10.1016/j.applthermaleng.2015.11.018.
[27] Freeman J, Hellgardt K, Markides CN. An assessment of solar-powered organic Rankine cycle systems for combined heating and power in UK domestic applications. Appl Energy 2015;138:605–20. doi:10.1016/j.apenergy.2014.10.035.
[28] Quoilin S, Orosz M, Hemond H, Lemort V. Performance and design optimization of a low-cost solar organic Rankine cycle for remote power generation. Sol Energy 2011;85:955–66. doi:10.1016/j.solener.2011.02.010.

[29] Casartelli D, Binotti M, Silva P, Macchi E, Roccaro E, Passera T. Power Block Off-design Control Strategies for Indirect Solar ORC Cycles. Energy Procedia, vol. 69, Elsevier; 2015, p. 1220–30. doi:10.1016/j.egypro.2015.03.166.
[30] Bruno JC, López-Villada J, Letelier E, Romera S, Coronas A. Modelling and optimisation of solar organic rankine cycle engines for reverse osmosis desalination. Appl Therm Eng 2008;28:2212–26. doi:10.1016/j.applthermaleng.2007.12.022.
[31] Bocci E, Villarini M, Vecchione L, Sbordone D, Di Carlo A, Dell'Era A. Energy and Economic Analysis of a Residential Solar Organic Rankine Plant. Energy Procedia 2015;81:558–68. doi:10.1016/j.egypro.2015.12.135.
[32] Mehrpooya M, Ghorbani B, Hosseini SS. Thermodynamic and economic evaluation of a novel concentrated solar power system integrated with absorption refrigeration and desalination cycles. Energy Convers Manag 2018;175:337–56. doi:10.1016/J.ENCONMAN.2018.08.109.
[33] Boyaghchi FA, Heidarnejad P. Thermoeconomic assessment and multi objective optimization of a solar micro CCHP based on Organic Rankine Cycle for domestic application. Energy Convers Manag 2015;97:224–34. doi:10.1016/j.enconman.2015.03.036.
[34] Karellas S, Braimakis K. Energy-exergy analysis and economic investigation of a cogeneration and trigeneration ORC-VCC hybrid system utilizing biomass fuel and solar power. Energy Convers Manag 2016;107:103–13. doi:10.1016/j.enconman.2015.06.080.
[35] Villarini M, Bocci E, Di Carlo A, Sbordone D, Falvo MC, Martirano L. Technical-economic analysis of an innovative small scale solar thermal - ORC cogenerative system. Lect. Notes Comput. Sci. (including Subser. Lect. Notes Artif. Intell. Lect. Notes Bioinformatics), vol. 7972 LNCS, 2013, p. 271–87.
[36] Cioccolanti L, Tascioni R, Bocci E, Villarini M. Parametric analysis of a solar Organic Rankine Cycle trigeneration system for residential applications. Energy Convers Manag 2018;163:407–19. doi:10.1016/J.ENCONMAN.2018.02.043.
[37] Innova-Microsolar n.d.
[38] Ahlgren B, Tian Z, Perers B, Dragsted J, Johansson E, Lundberg K, et al. A simplified model for linear correlation between annual yield and DNI for parabolic trough collectors. Energy Convers Manag 2018;174:295–308. doi:10.1016/J.ENCONMAN.2018.08.008.
[39] Mohammadi K, Goudarzi N. Association of direct normal irradiance with El Niño Southern Oscillation and its consequence on concentrated solar power production in the US Southwest. Appl Energy 2018;212:1126–37. doi:10.1016/j.apenergy.2017.12.102.
[40] Cioccolanti L, Tascioni R, Arteconi A. Mathematical modelling of operation modes and performance evaluation of an innovative small-scale concentrated solar organic Rankine cycle plant. Appl Energy 2018;221:464–76. doi:10.1016/j.apenergy.2018.03.189.
[41] Kloben n.d.
[42] Yazaki Energ Systems, Inc. n.d.
[43] Therminol ® 62 Heat Transfer Fluid n.d. http://www.therminol.com/products/Therminol-62 (accessed August 28, 2017).
[44] Pili P (Elianto). Elianto (Concentrating Solar Power) n.d. http://www.eliantocsp.it (accessed May 25, 2018).
[45] Enogia SAS. Enogia n.d. http://www.enogia.com/ (accessed May 25, 2018).
[46] 3M. Novec™ 649 n.d. https://www.3m.com/3M/en_US/company-us/all-3m-products/~/3M-Novec-649-Engineered-Fluid/?N=5002385+3290667401&rt=rud (accessed May 25, 2018).
[47] Thermacore. Aavid Thermacore n.d. https://www.thermacore.com/ (accessed May 25,

2018).

[48] Maldonado J, Fullana-Puig M, Martín M, Solé A, Fernández Á, de Gracia A, et al. Phase Change Material Selection for Thermal Energy Storage at High Temperature Range between 210 °C and 270 °C. Energies 2018;11:861. doi:10.3390/en11040861.

[49] Serrano-López R, Fradera J, Cuesta-López S. Molten salts database for energy applications. Chem Eng Process 2013. doi:10.1016/j.cep.2013.07.008.

[50] S.TRA.TE.G.I.E. S.TRA.TE.G.I.E. n.d. http://www.strategiesrl.com/ (accessed May 25, 2018).

[51] TRNSYS – Transient System Simulation Tool n.d. http://www.trnsys.com/ (accessed August 28, 2017).

[52] Matlab Mathworks n.d. https://www.mathworks.com/products/matlab.html (accessed August 28, 2017).

[53] Gantenbein P, Jaenig D, Kerskes H, Van Essen M. Final report of Subtask B " Chemical and Sorption Storage " The overview A Report of IEA Solar Heating and Cooling programme -Task 32 Advanced storage concepts for solar and low energy buildings Report B7 of Subtask B 2008.

[54] Richardson I, Thomson M, Infield D, Clifford C. Domestic electricity use: A high-resolution energy demand model. Energy Build 2010;42:1878–87. doi:10.1016/J.ENBUILD.2010.05.023.